Journal of Power Sources 268 (2014) 634–639

Contents lists available at ScienceDirect

Journal of Power Sources

journal homepage: www.elsevier.com/locate/jpowsour

Electrochemical performance and stability of lanthanum strontium cobalt ferrite oxygen electrode with gadolinia doped ceria barrier layer for reversible solid oxide fuel cell

Hui Fan [a,b], Michael Keane [b], Prabhakar Singh [b], Minfang Han [a,*]

[a] Union Research Center of Fuel Cell, School of Chemical & Environment Engineering, China University of Mining & Technology, Beijing 100083, China
[b] University of Connecticut, Center for Clean Energy Engineering, 44 Weaver Rd., Storrs, CT 06269-5233, United States

HIGHLIGHTS

- An LSCF oxygen electrode was prepared for RSOFCs with a GDC barrier layer.
- The barrier layer has a honeycomb-like structure.
- Repeated discharge/charge cycles of the cell were investigated.
- Delamination of the barrier layer from the YSZ electrolyte induces cell degradation.

ARTICLE INFO

Article history:
Received 20 December 2013
Received in revised form
15 March 2014
Accepted 18 March 2014
Available online 13 April 2014

Keywords:
Lanthanum strontium cobalt ferrite
Gadolinia doped ceria
Reversible solid oxide fuel cell
Solid oxide electrolysis cell

ABSTRACT

A $La_{0.6}Sr_{0.4}Co_{0.2}Fe_{0.8}O_{3-\delta}$ (LSCF) oxygen electrode and a $Gd_{0.1}Ce_{0.9}O_{2-\delta}$ (GDC) barrier layer are prepared for a reversible solid oxide fuel cell (RSOFC). Scanning electron microscopy (SEM) analysis shows that the GDC barrier layer has a honeycomb-like structure and maintains good adhesion with yttria-stabilized zirconia (YSZ) electrolyte and LSCF oxygen electrode. Polarization curves and electrochemical impedance spectra for both fuel cell and steam electrolysis modes are investigated. Repeated fuel cell/steam electrolysis cycles operated at 300 mA cm^{-2} and 800 °C shows the cell has higher degradation under steam electrolysis mode than under fuel cell mode. Cell degradation in electrolysis mode is attributed to delamination of the GDC barrier layer from the YSZ electrolyte, which has been observed during post-test SEM analysis.

1. Introduction

Hydrogen gas as a clean fuel has attracted extensive attention due to limited fossil fuel sources, increased oil prices, and environmental considerations. However, its production and storage is one of the major concerns. A reversible solid oxide fuel cell (RSOFC) is an electrochemical device capable of both generating electricity from fuel (SOFC) and generating fuel from electrolysis of steam and CO_2 (solid oxide electrolysis cell, SOEC). RSOFCs have attracted increased interest in the development of environmentally friendly methods of energy storage and electricity generation [1–3]. A variety of power sources such as nuclear power, wind power, solar energy, and waste heat from high temperature industrial process can be used for high temperature electrolysis process (SOEC mode) to produce hydrogen gas, which is subsequently stored and used in SOFCs to generate electricity and heat (SOFC mode) [4,5].

For SOFCs, yttria stabilized zirconia (YSZ) and nickel–YSZ (Ni–YSZ) are the most widely used electrolyte and anode materials, respectively. The YSZ and Ni–YSZ materials can also be employed in SOECs, exhibiting good electrochemical performance and stability [6,7]. The perovskite material LSM (lanthanum strontium manganite) used as an oxygen electrode is subject to delamination from the electrolyte, causing performance degradation and cell failure in SOECs [8–10]. Therefore, it is essential to develop materials for oxygen electrodes with high electrochemical performance and stability for both SOFCs and SOECs.

Oxygen electrode materials with high activity for oxygen reduction have been developed. Mixed ionic electronic conduction (MIEC) oxides have been studied based on thermodynamics and experiments, to simultaneously provide high electronic and ionic conductivity and high oxygen electrochemical reduction activity. Among the materials, Co-based perovskite materials could have

* Corresponding author.
E-mail address: hanminfang@sina.com (M. Han).

http://dx.doi.org/10.1016/j.jpowsour.2014.03.080
0378-7753/

potential for oxygen electrode in SOECs, but they suffer from the drawback of reaction with YSZ electrolyte at high temperature (>1000 °C) to form secondary phases such as $La_2Zr_2O_7$ and $SrZrO_3$ [11,12]. By applying a thin barrier layer of another electrolyte material, such as GDC (gadolinia doped ceria) [13,14], SDC (samaria doped ceria) [2,15], or YDC (yttria doped ceria) [16–18], the interfacial reaction between YSZ electrolyte and Co-based perovskite oxygen electrode can be inhibited [19]. Among the barrier materials, GDC presents the highest ionic conductivity.

$La_{1-x}Sr_xCo_{1-y}Fe_yO_3$ provides rapid surface exchange kinetics, high oxygen vacancy concentration, and mixed conductivity, and is widely used as a cathode material in SOFCs. LSCF electrodes have been explored to yield low-current interfacial resistance values that are a factor of 10 lower than for (La, Sr)MnO_3 cathodes [20]. Additionally, a barrier layer is introduced between the LSCF electrode and YSZ electrolyte to improve the stability of a cell by enhancing the compatibility at the interface [21]. A study by Laguna-Bercero et al. [22] has shown that LSCF was tested as an alternative reversible electrode in 10Sc1CeSZ (scandia and ceria stabilized zirconia) based cells, to assure good catalytic activity for oxygen reduction in fuel cell mode and oxygen evolution in electrolysis mode. It can be noted that LSCF is a good candidate as a reversible oxygen electrode using scandia stabilized zirconia (ScSZ) based cells. Nanocrystalline LSCF powder has been prepared with single perovskite phase for Ni–YSZ/YSZ/LSCF cell, with high peak-power density [23]. However, further studies are required to characterize the long-term stability of these cells. Jun Ko et al. [24] investigated a $(La_{0.6}Sr_{0.4})(Co_{0.2}Fe_{0.8})O_3$(LSCF)–$Y_{0.08}Zr_{0.92}O_{1.96}$(YSZ)–$Gd_{0.1}Ce_{0.9}O_{2-\delta}$(GDC) dual composite cathode for SOFCs, which showed low electrode polarization and high performance. The improvement of the cathodic performance is contributing to the use of LSCF materials, which have high electronic conductivity and ionic conductivity. LSCF cathodes combined with Ni–YSZ anodes and YSZ electrolyte for SOFCs have also been demonstrated to exhibit good electrochemical performance, with reduced cathode polarization resistances [25].

Besides the demand for electricity generation under fuel cell mode, there is growing interest in production of hydrogen from water splitting through an SOEC [26,27]. High temperature steam and/or CO_2 electrolysis has been developed and researched in recent years [28,29]. Furthermore, LSCF composite material can be employed into SOECs, as well as SOFCs for oxygen electrodes. LSCF–GDC as an oxygen electrode for the Ni–YSZ hydrogen electrode-supported electrolysis cells was capable of working reversibly in either fuel cell or electrolysis mode [30]. Use of LSCF1982 ($La_{0.1}Sr_{0.9}Co_{0.8}Fe_{0.2}O_{3-\delta}$) and LSCF1982-GDC composite oxygen electrodes with GDC barrier layer for YSZ electrolyte-based RSOCs has been reported by Moon-Bong Choi et al. [21]. It was indicated that cells with LSCF1982 oxygen electrodes exhibited better SOFC/SOEC performance than those with LSCF1982–GDC composite oxygen electrode. For co-electrolysis of H_2O and CO_2 mixture, LSCF–GDC oxygen electrodes showed lower overall degradation, and more stable electrochemical performance than LSM–YSZ electrodes [31].

Previous studies [2,21] on LSCF composite materials have suggested that the introduction of barrier layer between YSZ electrolyte and LSCF electrode can improve electrochemical performance and stability of SOFCs, as well as SOECs. However, few researchers are focused on the degradation mechanism of RSOFCs employing LSCF oxygen electrode and a barrier layer. In this study, the electrochemical performance of a hydrogen electrode-supported Ni–YSZ/YSZ/GDC/LSCF cell with an LSCF oxygen electrode and a GDC barrier layer was investigated under both fuel cell and steam electrolysis modes. Repeated fuel cell/steam electrolysis cycle performance of the cell was carried out as well for evaluating the cell stability. Degradation mechanism of the RSOFC is proposed based on post-test scanning electron microscopy (SEM) analysis.

2. Experimental

2.1. Powder preparation LSCF and GDC

LSCF ($La_{0.6}Sr_{0.4}Co_{0.2}Fe_{0.8}O_{3-\delta}$) powder was synthesized by a solution combustion method. As mentioned in previous work [23,32], stoichiometric amounts of $La(NO_3)_3 \cdot 6H_2O$ (analytical reagent grade, Beijing Chemical Reagent Company, China, the same below), $Sr(NO_3)_2$, $Co(NO_3)_2 \cdot 6H_2O$ and $Fe(NO_3)_3 \cdot 9H_2O$ were dissolved into deionized water. After it was stirred thoroughly, glycine (NH_2CH_2COOH) was then added at a molar ratio of 2.5:1 to the total metal ions to obtain precursor solution, which was subsequently heated and concentrated at 80 °C to yield gel. Further heating was performed at 180 °C to reach spontaneous ignition, to obtain precursor powder. The as-ignited powder was calcined in high-temperature furnace at 800 °C for 2 h in order to eliminate carbonaceous residues and to finally obtain LSCF powder.

GDC ($Gd_{0.1}Ce_{0.9}O_{2-\delta}$) powder was prepared by co-precipitation method and characterized as described in our previous work [33,34]. Cerium and gadolinium nitrate pentahydrate were used as starting materials, and ammonia and hydrogen peroxide were employed as the precipitants. The mixed salt solution was sprayed into a double volume of ammonia/hydrogen peroxide mixed solution until pH ≈ 8–9, which was then heated at 80–90 °C to turn to faint yellow. The precursor was washed repeatedly with deionized water and ethanol, dried, and calcined at 600 °C for 2 h, to finally produce GDC powder.

2.2. Fabrication of single RSOFC

The RSOFC single cells investigated in the study consisted of Ni–YSZ hydrogen electrode supports, thin YSZ electrolytes, GDC barrier layers, and LSCF oxygen electrodes. The support and electrolyte were fabricated by tape casting processes, and the barrier layer and the oxygen electrode were deposited on the electrolyte by screen printing techniques. Slurry for Ni–YSZ substrate was fabricated by ball-milling powders of NiO, YSZ (8 mol% yttria stabilized zirconia, with a median particle size of 0.114 μm) and graphite (Furunda Zirconium Material Co. Ltd., China) pore former in a weight ratio of 50:50:10 with appropriate amounts of ethanol-butanone solvent, caster oil dispersant, dibutyl phthalate (DBP) plasticizer, and polyvinyl butyral (PVB) binder. For YSZ electrolytes, the same method of slurry fabrication as in the case of NiO-YSZ substrates was used except that no NiO and graphite powders were added. A tape casting machine (DR-150, made in Japan) was used for separately casting the NiO–YSZ layer and the YSZ electrolyte. These tapes were dried in air at room temperature for 12 h. The green sheet of NiO–YSZ substrate (~300 μm) and the white YSZ electrolyte (20–30 μm) were stacked together under a vacuum condition and laminated at 20 MPa for 10 min using a thermal isostatic press (30T Shanxi, China) to form a NiO–YSZ supported half-cell. The resulting laminate was punched to discs, and then co-sintered in air at 1300 °C for 10 h in order to densify the electrolyte layer.

The ink slurry for the GDC barrier layer is composed of GDC powder, and ethyl cellulose (binder), and terpineol (solvent). This mixture was ball milled for 12 h with as-prepared organic vehicle in a 70:30 weight ratio to the homogeneous GDC slurry. Thus the obtained GDC printing ink was screen-printed on the pre-sintered YSZ electrolyte by a rubber squeegee. After sintering at 1300 °C in air for 2 h, the resulting barrier layer was about 10 μm thick.

The procedure for printing the LSCF oxygen electrode film was similar to that of printing the barrier layer. The ink slurry which was composed of LSCF and an organic vehicle in a weight ratio of 50:50 was screen printed on top of the GDC barrier layer. The LSCF layer

was sintered at 1200 °C in air for 2 h. Thickness of the LSCF was 60–70 μm.

2.3. Cell characterization and electrochemical measurements

Single RSOFC was sealed on an alumina tube as described elsewhere [35], using ceramic paste as sealant (Aramco-552, USA). The area of electrolyte and hydrogen electrode was about 1.5 cm^2, the external area of oxygen electrode was 0.2 cm^2, and Ag paste was used as the current collector. Silver wires were pressed against the oxygen electrode to obtain sufficient electronic contact with both electrodes in four-wire set up. The NiO–YSZ hydrogen electrode substrate was in-situ reduced in a tube furnace during start up and at 700 °C for 2 h in low-flow-rate H_2 atmosphere, and then the cell was tested at temperatures from 750 °C to 850 °C in both fuel cell and steam electrolysis modes. For SOFC testing, 80 sccm flow rate of humidified hydrogen gas (3% H_2O, volume fraction, the same below) was fed to the hydrogen electrode, while the oxygen electrode was exposed to ambient air. For SOEC operation, 50% H_2O, 25% H_2 and 25% Ar at a total flow rate of 150 sccm were introduced into the Ni-based hydrogen electrode by bubbling hydrogen and argon through deionized water at 81.5 °C. Similarly, the oxygen electrode was left open to atmospheric environment. Polarization curves and electrochemical impedance spectra (EIS) under open circuit were measured using an IM6 Electrochemical Workstation (ZAHNER, Germany). For EIS test, the frequency range was from 100 mHz to 100 kHz and the AC (alternate current) amplitude was 20 mV. For polarization measurement, the recorded voltage range was from 2 V to 0.3 V. To understand the operational stability of the RSOC under SOFC and SOEC modes, the variation of voltage with time at a constant current of 0.3 A cm^{-2} was recorded at 800 °C using an Arbin test system (Arbin MSTAT4). Microstructures of the pre/post-test NiO-YSZ/YSZ/GDC/LSCF cells were investigated by a scanning electron microscope (SEM, JEOL, JSM 6700F). In addition, the phase formation of LSCF powder and GDC powder was verified by a high power X-ray diffractometer (XRD, PANalytical X'Pert PRO, Netherlands) using CuKα radiation.

3. Results and discussion

3.1. Physico-chemical characterization of RSOFCs

The XRD patterns of the $Gd_{0.1}Ce_{0.9}O_{2-\delta}$ and $La_{0.6}Sr_{0.4}Co_{0.2}Fe_{0.8}O_{3-\delta}$ powders are shown in Fig. 1. For reference, XRD diffractions of pure GDC and LSCF powders are also displayed. The XRD profile in Fig. 1(a) shows that all peaks match the reference well and the as-prepared GDC powder clearly has the diffraction lines of a cubic fluorite structure. It is obvious that high purity solid solution phase of the GDC was produced. Thus, the diffractions of the $Gd_{0.1}Ce_{0.9}O_{2-\delta}$ powder display highly crystalline when sintered at 600 °C. In Fig. 1(b), the XRD spectrum indicates that the synthesized LSCF powder is the perovskite-type structure after calcining at 800 °C for 2 h. This demonstrates that the present solution combustion method yields $La_{0.6}Sr_{0.4}Co_{0.2}Fe_{0.8}O_{3-\delta}$ oxide.

3.2. SEM images of cross-sectional view for RSOFC

Typical cross-sectional micrographs of the NiO–YSZ/YSZ/GDC/LSCF RSOFC and the barrier layer-electrolyte interface are shown in Fig. 2(a) and (b), respectively. In Fig. 2(a), the YSZ electrolyte with thickness of ~20 μm, exhibits a fully dense microstructure without pores or cracks. Both the hydrogen and oxygen electrode layers display a highly porous microstructure, and have the thickness of ~300 μm and 60–70 μm, respectively. As shown in Fig. 2(b), the GDC barrier layer sintered at 1300 °C has a honeycomb-like structure, but maintains good adhesion between the YSZ electrolyte layer and LSCF oxygen electrode. Thickness of the GDC barrier layer is approximately 7–10 μm. GDC has been reported to be dense at a sintering temperature of 1500 °C [36]. By reducing the sintering temperature of the GDC barrier layer, the YSZ electrolyte avoids high temperature-induced larger grain formation [37], simultaneously ensuring tight adherence with the porous GDC layer.

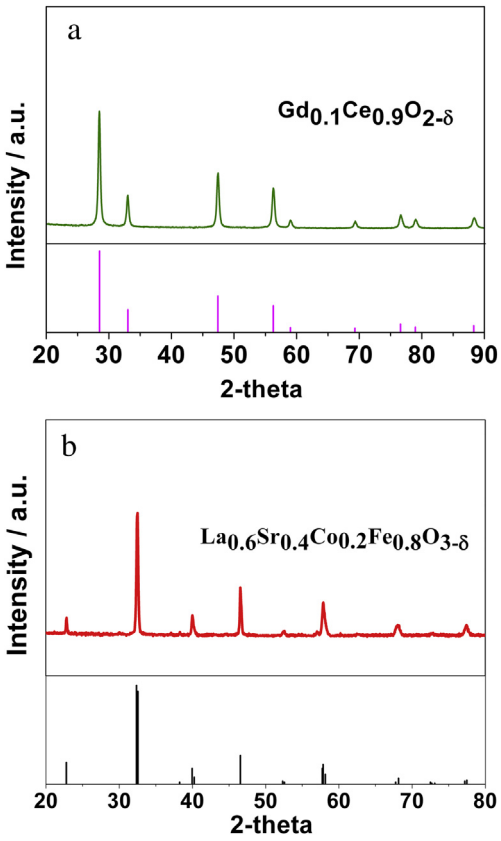

Fig. 1. X-ray diffraction patterns of (a) GDC powder calcined at 600 °C and (b) LSCF powder prepared by sintering at 800 °C.

3.3. Initial electrochemical characterization under SOFC mode

The Nernst equation (Eq. (1)) provides the theoretical open circuit voltage (OCV) based on temperature and atmospheric conditions.

$$E = E_0 - \frac{nF}{RT}\ln\frac{P_{H2O}}{P_{H2}*(P_{O2})^{1/2}} \quad (1)$$

where E_0 is the standard electrode potential, R is the universal gas constant, T is the absolute temperature (in Kelvin), F is the Faraday constant, P_{H2} and P_{H2O} denote the partial pressure of hydrogen and steam, respectively, at the hydrogen electrode side, and P_{O2} denotes the partial pressure of oxygen (0.21 atm) at the oxygen electrode side.

The initial performance of the Ni–YSZ/YSZ/GDC/LSCF button cells was evaluated in SOFC mode. Fig. 3(a) shows the voltage and power density vs current density (V–I and P–I) characteristic curves at 850 °C to 750 °C, and the measurement was programmed to stop at a cell voltage below 0.3 V. The operating conditions were 97% H_2 and 3% H_2O at a flow rate of 80 sccm as a fuel feed and air as an oxidant. The OCV of the cell is 1.086 V, 1.093 V, and 1.102 V at 850 °C, 800 °C, and 750 °C, respectively. These values are very close

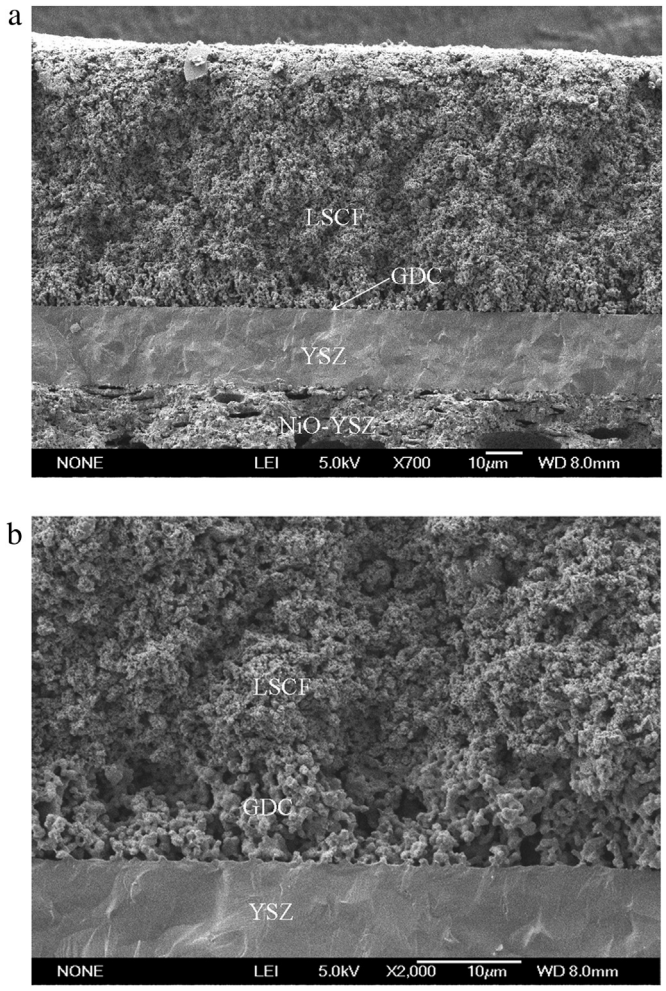

Fig. 2. Typical SEM images for cross-sectional views of (a) the freshly prepared NiO–YSZ/YSZ/GDC/LSCF cell, and (b) the NiO/YSZ–GDC interface.

to the theoretical OCVs obtained from the Nernst equation (Eq. (1)), implying the YSZ electrolyte layer is fully dense after sintering at 1300 °C and there is no leakage between the cell and the alumina tube. It is also shown that the OCVs of the cell are increased with decreasing test temperature, which agrees well with the Nernst equation.

The maximum power densities of the cell are approximately 486 mW cm^{-2}, 401 mW cm^{-2}, and 296 mW cm^{-2} at 850 °C, 800 °C, and 750 °C, respectively. Leone et al. [25] have demonstrated that LSCF was really effective for decreasing the electrode activation polarization for solid oxide fuel cells. The cell shows the best performance at 850 °C, since operation at high temperature results in low electrode polarization resistance and high electrolyte conductivity [38].

Fig. 3(b) shows the impedance spectra results of the Ni-YSZ/YSZ/GDC/LSCF cell under open circuit at 850 °C to 750 °C. It is observed that the ohmic resistance of the cell, determined from the high-frequency intercept on the real axis, was 0.35 Ω cm^2, 0.43 Ω cm^2 and 0.56 Ω cm^2 at 850 °C, 800 °C, and 750 °C, respectively. These ohmic resistances are much larger than those reported by Chen et al. [39] and may not be from electrolyte contribution alone. In addition, interfacial resistance, electrode resistance, and contact resistance are also important contributions. The electrode polarization resistance of the cell, determined from the differences between high- and low-frequency intercepts on real axis of the impedance spectra, was 0.87 Ω cm^2, 0.96 Ω cm^2, and 1.39 Ω cm^2 at 850 °C, 800 °C, and 750 °C, respectively. For a fuel cell application, the total resistances of this cell operating at 850 °C–750 °C are large. Hence, further scope is remained in decreasing total resistances through optimization of fabrication parameters. Compared to LSM, LSCF material has a higher vacancy concentration and better catalytic activity for oxygen reduction during cathode reaction, resulting in lower electrode polarization resistance [40]. LSCF has been investigated to be a good oxygen electrode material in SOFC, with high catalytic activity for oxygen reduction [21]. Constantin et al. [13] have reported that a GDC buffer layer sandwiched between LSCF and YSZ for SOFCs blocked strontium diffusion and reduced series and polarization resistance, consequently limiting the interface degradation.

3.4. Electrochemical performance under SOEC mode

The electrochemical performance of the single cell with LSCF as oxygen electrode and GDC as barrier layer measured under SOEC mode at 750 °C–850 °C is shown in Fig. 4. 50% H_2O, 25% H_2 and 25% Ar as inlet gas with a total flow rate of 150 sccm was fed to the Ni/YSZ hydrogen electrode. Fig 4(a) shows the typical voltage (V) versus current density (I) curves for the Ni–YSZ/YSZ/GDC/LSCF cell recorded in steam electrolysis mode starting from OCV. The measured OCVs are nearly the same as the theoretical value predicted from Nernst equation (Eq. (1)). For the V–I curves, it can be observed that the electrolysis voltage increases with increasing current density. When the temperature is increased, the slope of V–I curves decreases and the current density increases, which

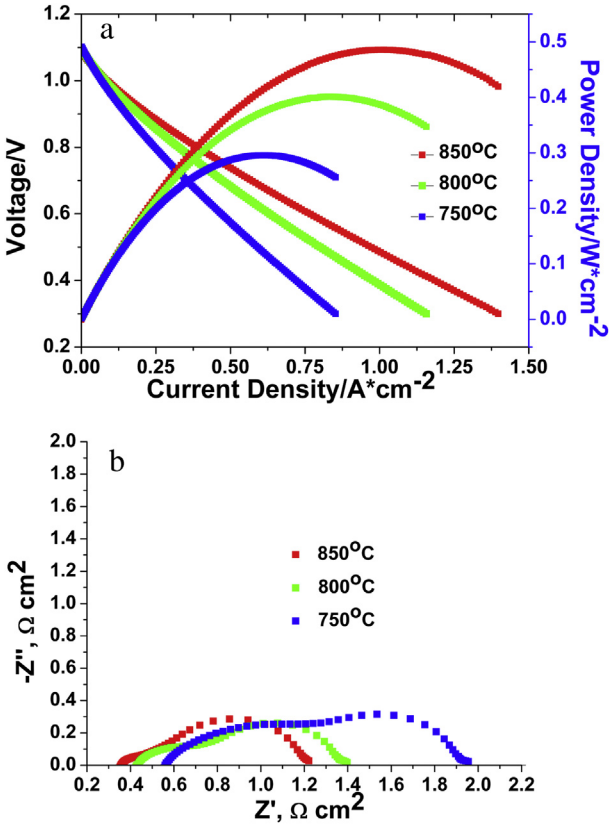

Fig. 3. (a) Voltage and power density vs current density, and (b) electrochemical impedance spectra (EIS) at open circuit at 850 °C–750 °C for Ni–YSZ/YSZ/GDC/LSCF cell under SOFC mode operated with a 97% H_2 and 3% H_2O mixture at 80 sccm in the hydrogen electrode and ambient air in the oxygen electrode.

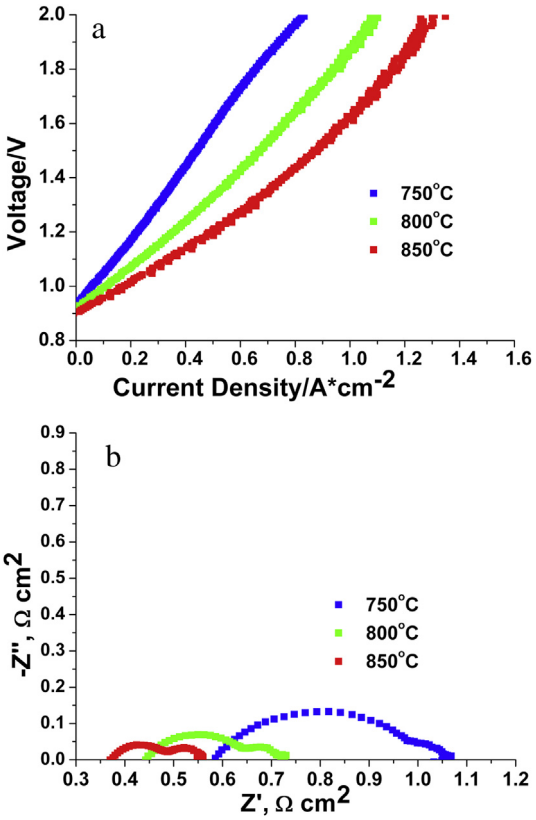

Fig. 4. (a) Voltage vs current density, and (b) electrochemical impedance spectra at open circuit at 750 °C–850 °C for Ni–YSZ/YSZ/GDC/LSCF cell under SOEC mode operated with a 50% H_2O, 25% H_2 and 25% Ar gas mixture at 150 sccm in the hydrogen electrode and ambient air in the oxygen electrode.

indicates lower electrolysis voltage is required for the hydrogen production. For example, for a voltage of 1.3 V, current densities of 0.30 A cm^{-2}, 0.47 A cm^{-2}, and 0 63 A cm^{-2} have been measured at 750 °C, 800 °C, and 850 °C, respectively. The improvement in the hydrogen production with the increase in temperature could be attributed to the reduction in energy loss associated with the polarization of electrode and lower electrolyte ionic resistance [21].

Fig. 4(b) shows EIS response of the LSCF–oxygen electrode cell at OCV condition during SOEC operation at different temperatures. In steam electrolysis mode, the electrode polarization resistance is mainly attributed to the charge transfer reaction at the electrode/electrolyte interface, the adsorption/desorption, and diffusion inside the porous electrode [30]. As shown in Fig. 4(b), ohmic resistance of the LSCF electrode-cell at OCV under SOEC mode is 0.37 Ω cm^2, 0.43 Ω cm^2, and 0.58 Ω cm^2 at 850 °C, 800 °C, and 750 °C, respectively. These ohmic resistance values are about the same as for fuel cell mode. The polarization resistances of the cell are 0.19 Ω cm^2, 0.26 Ω cm^2, and 0.5 Ω cm^2 are at 850 °C, 800 °C, and 750 °C, respectively. It can be noted that the difference in cell performance in the two modes is primarily due to the different inlet gas composition for the two cases. Choi et al. [21] have reported that polarization resistance for a button cell with LSCF1982 oxygen electrode and GDC barrier layer in SOEC mode was 0.244 Ω cm^2, nevertheless the ohmic resistance was as low as 0.049 Ω cm^2. The low ohmic resistance is due to small thickness of electrolyte (6–10 μm) and the use of NiO–YSZ functional layer between hydrogen electrode and electrolyte, which increases the TPB (triple phase boundary) area. The comparable results have shown that LSCF can be presented as a good candidate for oxygen electrodes for SOEC operation.

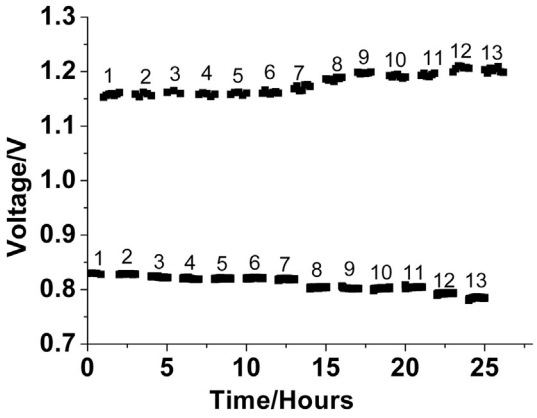

Fig. 5. Fuel cell/steam electrolysis cycle of Ni–YSZ/YSZ/GDC/LSCF cell at 300 mA cm^{-2} and 800 °C.

3.5. Fuel cell/steam electrolysis cycle

The stability of LSCF oxygen electrodes and GDC barrier layer for RSOFCs was characterized by charge/discharge cycle. Fig. 5 shows repeated charge/discharge cycle performance (1 h of steam electrolysis and 1 h of fuel cell mode each) of the Ni–YSZ/YSZ/GDC/LSCF cell at 300 mA cm^{-2} and 800 °C. During 13 cycles, the discharge voltage was gradually decreased from 0.827 V to 0.806 V and the charge voltage increased from 1.122 V to 1.189 V. The corresponding voltage degradation of the cell is 2.7% and 5.9% for fuel cell mode and electrolysis mode, respectively. Only few of the results on reversible RSOFC reported in literature include repeated charge/discharge cycle, therefore, it is difficult to make a comparison of the testing data presented here with results for a similar test. However, in view of the degradation of the RSOFC during repeated charge/discharge cycles for 13 times, it is necessary to find evidence for improvement of long-term durability.

3.6. Pre- and post-test microstructure observation at the GDC/YSZ interface

Fig. 6 shows the SEM images of cross-section of GDC barrier layer/YSZ electrolyte interface for the NiO–YSZ/YSZ/GDC/LSCF cell before and after fuel cell/steam electrolysis cycles at 300 mA cm^{-2} and 800 °C. The YSZ electrolyte surface in good contact with GDC barrier layer for a freshly prepared cell is shown in Fig. 6(a), and this can also be indicated by Fig. 2(b). After discharge/charge cycles at 300 mA cm^{-2} and 800 °C for 13 times, the GDC barrier layer was found to be delaminated from the YSZ electrolyte (Fig. 6(b)). Fig. 6(c) shows gap formation between the YSZ electrolyte and GDC barrier layer in comparison with Fig. 2(b). The delamination may be the cause of cell deterioration during the repeated discharge/charge cycles.

4. Conclusions

An LSCF oxygen electrode and a GDC barrier layer were developed for preparing Ni–YSZ/YSZ/GDC/LSCF RSOFC cell. The electrochemical performance of the RSOFC was investigated in both fuel cell and steam electrolysis modes using polarization curves and electrochemical impedance spectroscopy. In constant galvanostatic discharge/charge conditions, the cells had higher performance degradation (5.9%) under electrolysis mode than under fuel cell mode (2.7%). After 13 repeated discharge/charge cycles, microstructure analysis of the post-test cell determined that the

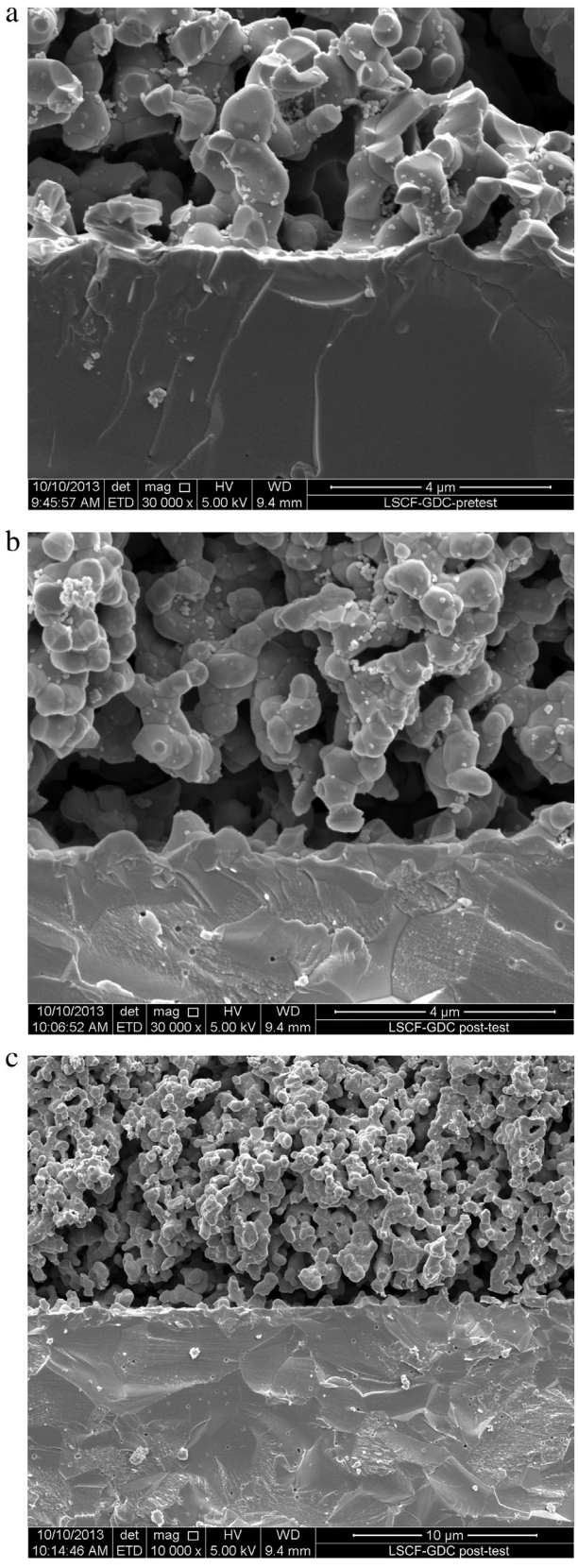

Fig. 6. SEM images of cross-section of GDC barrier layer/YSZ electrolyte interface for the NiO–YSZ/YSZ/GDC/LSCF cell (a) before, and (b) (c) after fuel cell/steam electrolysis cycle at 300 mA cm^{-2} and 800 °C.

deterioration was probably due to delamination of the GDC barrier layer from the YSZ electrolyte.

Acknowledgements

We are grateful to National Basic Research Program of China (973 Program No. 2012CB215404, No. 2012CB215404), and China Scholarship Council (No. 201306430012) for financial support of this work.

References

[1] S. Gopalan, G. Ye, U.B. Pal, J. Power Sources 162 (2006) 74–80.
[2] Y. Tao, H. Nishino, S. Ashidate, H. Kokubo, M. Watanabe, H. Uchida, Electrochim. Acta 54 (2009) 3309–3315.
[3] G.-B. Jung, J.-Y. Chen, C.-Y. Lin, S.-Y. Sun, Int. J. Hydrogen Energy 37 (2012) 15801–15807.
[4] G.B. Chen, H.M. Zhang, H.X. Zhong, H.P. Ma, Electrochim. Acta 55 (2010) 8801–8807.
[5] Y.Y. Rao, Z.Q. Wang, W. Zhong, R.R. Peng, Y.L. Lu, J. Power Sources 199 (2012) 142–145.
[6] K.F. Chen, N. Ai, S.P. Jiang, Int. J. Hydrogen Energy 37 (2012) 10517–10525.
[7] P. Kim-Lohsoontorn, D.J.L. Brett, N. Laosiripojana, Y.-M. Kim, J.-M. Bae, Int. J. Hydrogen Energy 35 (2010) 3958–3966.
[8] J. Kim, H.-I. Ji, H.P. Dasari, D. Shin, H. Song, J.-H. Lee, B.-K. Kim, H.-J. Je, H.-W. Lee, K.J. Yoon, Int. J. Hydrogen Energy 38 (2013) 1225–1235.
[9] M. Keane, M.K. Mahapatra, A. Verma, P. Singh, Int. J. Hydrogen Energy 37 (2012) 16776–16785.
[10] N. Li, M. Keane, M.K. Mahapatra, P. Singh, Int. J. Hydrogen Energy 38 (2013) 6298–6303.
[11] B. Yu, W.Q. Zhang, J.M. Xu, J. Chen, Int. J. Hydrogen Energy 33 (2008) 6873–6877.
[12] N. Li, A. Verma, P. Singh, J.-H. Kim, Ceram. Int. 39 (2013) 529–538.
[13] G. Constantin, C. Rossignol, P. Briois, A. Billard, L. Dessemond, E. Djurado, Solid State Ionics 249–250 (2013) 98–104.
[14] B.J. Ingram, J.A. Eastman, K.-C. Chang, S.K. Kim, T.T. Fister, E. Perret, H. You, P.M. Baldo, P.H. Fuoss, Appl. Phys. Lett. 101 (2012) 051603.
[15] H. Lin, C. Ding, K. Kumada, K. Sato, Y. Tsutai, C. Wada, T. Hashida, in: 5th International Workshop on Water Dynamics, AIP Conference Proceedings, vol. 987, 2008, pp. 54–57.
[16] S.-G. Kim, S.P. Yoon, S.W. Nam, S.-H. Hyun, S.-A. Hong, J. Power Sources 110 (2002) 222–228.
[17] R.R. Peng, C.R. Xia, X.Q. Liu, D.K. Peng, G.Y. Meng, Solid State Ionics 152–153 (2002) 561–565.
[18] Z. Fan, J. An, A. Iancu, F.B. Prinz, J. Power Sources 218 (2012) 187–191.
[19] W.Q. Zhang, B. Yu, J.M. Xu, Int. J. Hydrogen Energy 37 (2012) 837–842.
[20] E.P. Murray, M.J. Sever, S.A. Barnett, Solid State Ionics 148 (2002) 27–34.
[21] M.-B. Choi, B. Singh, E.D. Wachsman, S.-J. Song, J. Power Sources 239 (2013) 361–373.
[22] M.A. Laguna-Bercero, J.A. Kilner, S.J. Skinner, Solid State Ionics 192 (2011) 501–504.
[23] Z. Lei, Q.S. Zhu, L. Zhao, J. Power Sources 161 (2006) 1169–1175.
[24] H.J. Ko, J.-H. Myung, J.-H. Lee, S.-H. Hyun, J.S. Chung, Int. J. Hydrogen Energy 37 (2012) 17209–17216.
[25] P. Leone, M. Santarelli, P. Asinari, M. Calì, R. Borchiellini, J. Power Sources 177 (2008) 111–122.
[26] J.S. Herring, J.E. O'Brien, C.M. Stoots, G.L. Hawkes, J.J. Hartvigsen, M. Shahnam, Int. J. Hydrogen Energy 32 (2007) 440–450.
[27] J.E. O'Brien, ASME J. Heat. Transf. 134 (2012) 031017.
[28] S.H. Jensen, P.H. Larsen, M. Mogense, Int. J. Hydrogen Energy 32 (2007) 3253–3257.
[29] C.M. Stoots, J.E. O'Brien, J.S. Herring, J.J. Hartvigsen, ASME J. Fuel Cell Sci. Technol. 6 (2009) 011014.
[30] Z.L. Zhan, L. Zhao, J. Power Sources 195 (2010) 7250–7254.
[31] P. Hjalmarsson, X.F. Sun, Y.-L. Liu, M. Chen, J. Power Sources 223 (2013) 349–357.
[32] Ze Liu, M.-F. Han, W.-T. Miao, J. Power Sources 173 (2007) 837–841.
[33] M.-F. Han, S. Zhou, Z. Liu, Z. Lei, Z.-C. Kang, Solid State Ionics 192 (2011) 181–184.
[34] M.F. Han, Z. Liu, S. Zhou, L. Yu, J. Mater, Sci. Technol. 27 (2011) 460–464.
[35] H.-C. Yu, F. Zhao, A.V. Virkar, K.-Z. Fung, J. Power Sources 152 (2005) 22–26.
[36] C.J. Fu, Q.L. Liu, S.H. Chan, X.M. Ge, G. Pasciak, Int. J. Hydrogen Energy 35 (2010) 11200–11207.
[37] T. Talebi, M. Haji, B. Raissi, Int. J. Hydrogen Energy 35 (2010) 9420–9426.
[38] D. Rembelski, J.P. Viricelle, L. Combemale, M. Rieu, Fuel Cells 12 (2012) 256–264.
[39] Y. Chen, J. Bunch, C. Jin, C.H. Yang, F.L. Chen, J. Power Sources 204 (2012) 40–45.
[40] S. Lee, H.S. Song, S.H. Hyun, J. Kim, J. Moon, J. Power Sources 195 (2010) 118–123.